An energy balance of high-speed abrasive water jet erosion

A W Momber[1*,**] and **R Kovacevic**[2]
[1]WOMA Apparatebau GmbH, Duisburg, Germany
[2]Department of Mechanical Engineering, Southern Methodist University, Dallas, Texas, USA

Abstract: High-speed abrasive water jetting is an alternative tool for machining engineering materials. The energy dissipation processes involved in this erosion process have not been investigated systematically. In this paper, a model is developed to calculate the energy dissipation in workpieces eroded by abrasive water jets. By introducing an energy dissipation function $\chi(\Phi)$, the model enables the estimation of the energy absorption as a function of the erosion depth. The energy dissipation function can be expressed by a second-order polynomial approximation. Measurements of the reaction forces on the exiting slurry after the erosion process, material removal experiments and fracture tests are conducted to separate the components of the energy dissipation parameter, such as damping, friction and erosion debris generation.

Keywords: erosion, cutting, damping, friction

NOTATION

a, b	striation regression parameters
A, B, C	regression parameters
d^*	erosion debris size distribution parameter
d_F	focusing tube diameter
D	damping parameter
E_{diss}	terminal dissipated energy for $\Phi = 1$
E_{ex}	slurry exit kinetic energy
$E_{ex.T}$	slurry exit kinetic energy for $\Phi < 1$
E_{fr}	specific fracture energy
E_F	energy dissipated owing to friction
E_M	energy dissipated owing to material removal
E_S	slurry kinetic energy
F	friction parameter
F_{ex}	slurry exit reaction force
F_S	slurry reaction force
h	erosion depth
h_{max}	maximum erosion depth
K	constant
L	length of the erosion zone
$\dot{m}_P$	abrasive particle mass flowrate
m_S	slurry mass
$\dot{m}_W$	water mass flowrate
M	material removal parameter
n	erosion debris size distribution parameter
p	pump pressure
p_{thr}	critical threshold pressure
S_P	erosion debris surface
t	erosion time
v	traverse rate
v_{ex}	slurry exit flow velocity
v_S	slurry flow velocity
v_W	water flow velocity
V_M	eroded material volume
x	traverse coordinate
α	energy transfer coefficient
β	width of the erosion zone
Γ_M	work of fracture
ε	strain
ρ_W	water density
φ	velocity transfer coefficient
Φ	relative erosion depth
χ	energy absorption parameter
Ψ	energy dissipation due to other mechanisms

The MS was received on 13 March 1998 and was accepted after revision for publication on 4 December 1998.
* *Corresponding author: WOMA Apparatebau GmbH, PO Box 141820, D-47208 Duisburg, Germany.*
** *Visiting Professor at the Southern Methodist University, Dallas, Texas, USA.*

1 INTRODUCTION

High-speed abrasive water jetting is one of the most recently introduced machining methods. Using this technique, it is possible to cut all technical materials, including ceramics [**1**], alloys and composite materials [**2**]. As shown

in reference [**3**], this principle has the capability for milling and three-dimensional machining of materials, too.

An abrasive water jet is a high-speed multiphase mixture consisting of solid particles (abrasives), water and air. It is formed by accelerating the abrasive particles, usually garnet or aluminium oxide with diameters typically between 100 and 500 μm, through contact with a high-velocity plain water jet. The mixing between abrasives, water and air and the acceleration of the abrasives take place in a focusing tube as illustrated in Fig. 1. The abrasive particles leave the focusing tube with velocities of several hundred metres per second. A high number of abrasives (about 10^5 per second) leads to a high-frequency impingement on the processed surfaces [**3**, **4**]. Because of the small diameter of the focusing tube (typically 0.8–1.6 mm), the high-speed mixture acts like a streamline tool, similar to a laser or an electron beam, which is characterized by an unsteady material removal process in regard to the erosion depth.

Therefore, the most pronounced characteristic of surfaces generated by the high-speed abrasive–water flow is the presence of striation marks that begin below a relatively smooth region, as shown in Fig. 2. The origin of these striations is a controversial issue. Based on high-speed photographs taken from transparent materials, the idea of two different material removal mechanisms, called 'cutting wear' and 'deformation wear', has been introduced [**5**, **6**]. In the 'cutting wear' zone, the abrasive particles strike the material surface at shallow angles, producing a relatively smooth cutting surface. In the 'deformation wear' zone, unsteady removal with striation marks results from erosive wear due to particles impacting at large angles of attack. This model has been rejected by Raju and Ramulu [**7**] who found that, for a given material, the removal mechanism is independent of the erosion depth. The mechanisms may be different for different materials. These

Fig. 2 Typical striation marks formed during the high-speed abrasive water jet erosion (aluminium)

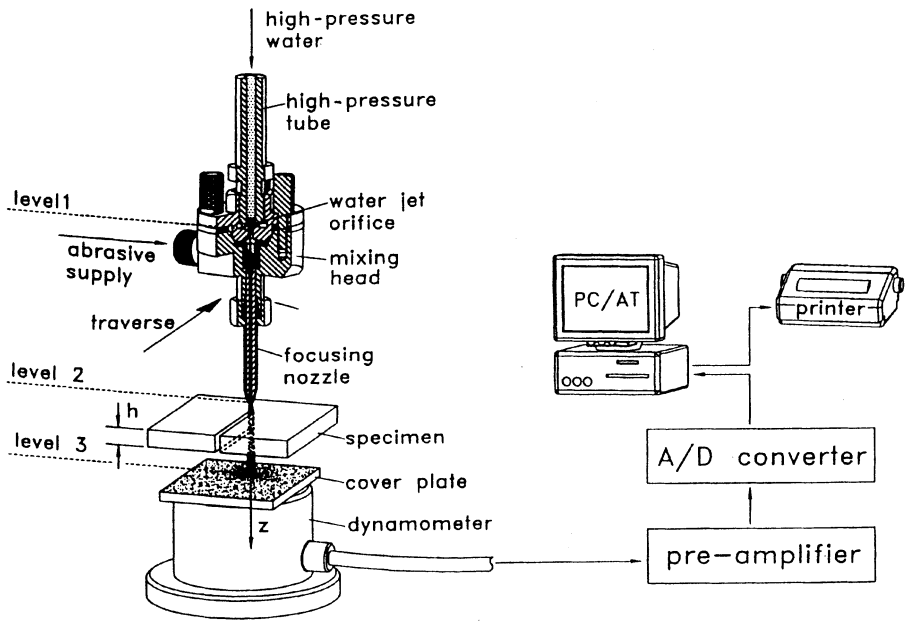

Fig. 1 A schematic diagram of abrasive waterjet formation and principle of the jet force measurements: A/D, analogue to digital

workers suggested that striations are produced on the cutting surface when the kinetic energy of the high-speed slurry flow falls below a certain critical kinetic energy. A similar idea was introduced in reference [**8**], based on roughness measurements. In contradiction to these findings, Chao and Geskin [**9**] discussed the unsteady removal process as a result of external disturbances, such as machine vibrations, but this concept does not cover observations on hard-to-machine materials. A global model for the three-dimensional unsteady cutting process has been suggested in reference [**10**].

A major contribution to this discussion is the quantification of the energy dissipation in the material during the erosion by a high-speed abrasive–water flow that allows the calculation of the local kinetic energy of the slurry flow at any specific erosion depth. This paper presents a mathematical model and experimental methods developed to quantify the energy dissipation during the erosion of materials by a high-speed slurry of abrasives and water.

2 GLOBAL MODELLING OF THE ENERGY DISSIPATED IN THE WORKPIECE

The kinetic energy of the high-speed slurry flow exiting from the focusing tube is

$$E_S = \tfrac{1}{2} m_S v_S^2 \tag{1}$$

With $m_S = (\dot{m}_P + \dot{m}_W)t$ and $t = d_F/v$, the equation is

$$E_S = \frac{d_F}{2v}(\dot{m}_P + \dot{m}_W)v_S^2 \tag{2}$$

Using a simple momentum transfer between the high-speed water flow in the focusing tube and the incoming solid particles (see Fig. 1), the velocity of the high-speed suspension can be approximated by

$$v_S = \alpha \frac{v_W}{1 + \dot{m}_P/\dot{m}_W} \tag{3}$$

Here, α is a mixing efficiency coefficient which can be estimated by force measurements. It depends strongly on the geometry of the focusing tube. Typical values measured by the present authors for different pump pressures and different abrasive mass flowrates are between $\alpha = 0.57$ and $\alpha = 0.71$ [**11**]. The velocity of the high-speed water flow, which is formed in an orifice (see Fig. 1), can be approximated by applying Bernoulli's law

$$v_W = \varphi \sqrt{\frac{2p}{\rho_W}} \tag{4}$$

Here, the parameter φ characterizes the energy transfer in the orifice and can be estimated by measuring the high-speed slurry impacting forces too [**11**]. Combining equations (1) to (4) gives

$$E_S = \frac{\alpha^2 \varphi^2 d_F(\dot{m}_P + \dot{m}_W)p}{(1 + \dot{m}_P/\dot{m}_W)^2 v \rho_W} \tag{5}$$

This energy is supplied to the erosion process and dissipated by different mechanisms, mainly by the generation of erosion debris, by the friction on the kerf walls and by the damping of the slurry due to a water–solid film on the local erosion site. A simple expression for the energy which contributes directly to the erosion is based on the assumption that part of the input energy leaves the material after the erosion process occurs, as shown in Fig. 3, even if the maximum possible erosion depth h_{max} is obtained. The difference between input energy and exit energy is equal to the energy dissipated in the material during the erosion process:

$$E_{diss} = E_S - E_{ex} \tag{6}$$

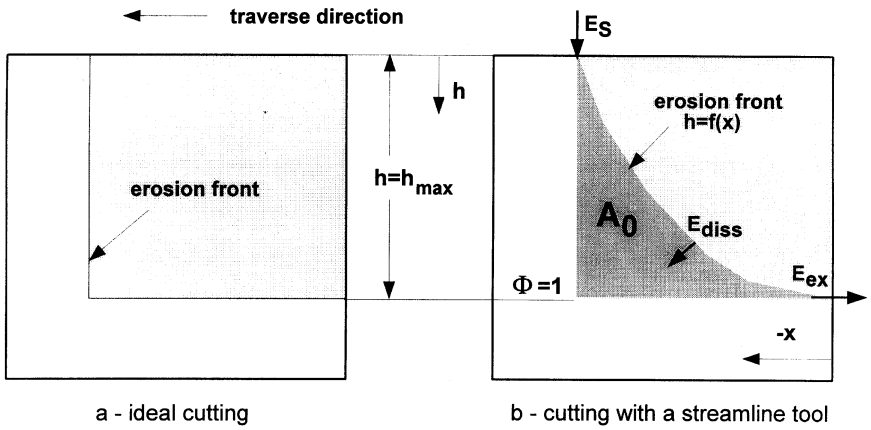

Fig. 3 Simplified energy balance during the erosion by high-speed abrasive–water flow and a schematic diagram of the energy dissipation during material cutting using a streamline tool

Keeping the input energy constant, the value of this energy depends only on the relative erosion depth. The relative erosion depth is

$$\Phi = \frac{h}{h_{\max}} \tag{7}$$

Thus,

$$E_{\text{diss}}(\Phi) = \chi(\Phi)(E_{\text{S}} - E_{\text{ex}}) \tag{8}$$

By definition, $\chi = 0$ for $\Phi = 0$, and $\chi = 1$ for $\Phi = 1$. Therefore, for $h = h_{\max}$, equation (8) is identical with equation (6) and, for $h = 0$, equation (8) gives $E_{\text{diss}} = 0$. It has been shown in many experiments that the erosion process is characterized by a critical process parameter, namely the threshold pressure p_{thr}, which has to be exceeded to initiate the erosion process [**4**]. It is assumed here that this critical pressure characterizes the exit energy of the high-speed slurry for $h = h_{\max}$ because, in the case when the maximum possible erosion depth is reached, the high-speed slurry leaves the material only if it is not able to remove more material. Therefore, from equation (5),

$$E_{\text{ex}} = K p_{\text{thr}} \tag{9}$$

The threshold pressure can be estimated experimentally by plotting the erosion depth versus the applied pump pressure. Combining equations (5), (8) and (9) gives

$$\begin{aligned} E_{\text{diss}}(\Phi) &= \chi(\Phi)\frac{\alpha^2\varphi^2 d_{\text{F}}(\dot{m}_{\text{P}} + \dot{m}_{\text{W}})}{v(1 + \dot{m}_{\text{P}}/\dot{m}_{\text{W}})^2\rho_{\text{W}}}(p - p_{\text{thr}}) \\ &= \chi(\Phi)K(p - p_{\text{thr}}) \end{aligned} \tag{10}$$

This equation gives the amount of energy which is dissipated in the workpiece during the erosion process at any particular erosion depth.

The parameter $\chi(\Phi)$ is assumed here to describe different mechanisms of energy dissipation, mainly

(a) energy dissipation due to erosion debris formation, denoted M,
(b) energy dissipation due to friction on the erosion kerf walls, denoted F,
(c) energy dissipation due to water–particle–film damping on the erosion site, denoted D and
(d) other mechanisms, such as heating, erosion debris acceleration and particle fragmentation, denoted Ψ.

Thus, $\chi(\Phi)$ can be written

$$\chi(\Phi) = M(\Phi) + F(\Phi) + D(\Phi) + \Psi(\Phi) \tag{11}$$

For further treatment, the portion Ψ is neglected. The following sections contain different experimental methods developed by the present authors to estimate the functions $\chi(\Phi)$, $M(\Phi)$, $F(\Phi)$ and $D(\Phi)$. The parameter conditions of the performed experiments are summarized in Table 1.

3 ESTIMATION OF THE BASIC ENERGY DISSIPATION FUNCTION $\chi(\Phi)$

The idea of using the geometry of the striations to estimate the energy dissipation function $\chi(h)$ was introduced by Momber and Kovacevic [**12**]. The basic assumption of this concept is given in Fig. 3. The shape of the striation can be modelled by a parabolic curve [**12**, **13**]. The area A_0 in Fig. 3 is given by

$$A_0 = \int_0^{x=b} [a(x-b)^2 + h_{\max}]\,\mathrm{d}x \tag{12}$$

Here, a and b are striation parameters which can be estimated by measuring the striation geometry (see Fig. 2). It is assumed that A_0 characterizes the energy dissipation up to the maximum possible erosion depth $h_{\max}$ under the given conditions. Therefore, $A_0 = A_{\max}$ for $\Phi = 1$. The energy dissipated up to any other certain depth is simply

Table 1 Parameter conditions for the experiments performed

			Types of experiment and target materials			
Parameter	Units	Symbol	Striation measurement; cast iron, ASTM 40, aluminium alloy 2024, titanium	Force measurement; aluminium alloy 2024	Fracture measurement; concrete	Grain size measurement; cast iron, ASTM 40
Pressure	MPa	p	276	100–250	100–350	140–350
Traverse rate	mm/s	v	0.42–1.06	0–2.0	2.0–12.0	4.2
Abrasive flowrate	g/s	$\dot{m}_{\text{P}}$	3.4	7.57–12.5	6.12–19.0	4.3
Orifice diameter	mm	d_0	0.254	0.254	0.457	0.33
Focus tube diameter	mm	d_{F}	0.50	0.50	1.27	1.02
Stand-off distance	mm	s	9.0	2.0–11.0	6.0	9.0
Impact angle	deg	ϕ	90			
Abrasive type	—	—	Garnet 80		Garnet 36	

expressed by the occupied area $A(\Phi)$, with $0 \leqslant A(\Phi) \leqslant A_0$. Therefore, the energy dissipation function is given by

$$\chi(\Phi) = \frac{A(\Phi)}{A_0} = \frac{A(\Phi)}{A(\Phi = 1)} \tag{13}$$

It can be seen that $\chi(\Phi) = 0$ for $h = 0$ $(\Phi = 0)$, and $\chi(\Phi) = 1$ for $h = h_{\max}$ $(\Phi = 1)$. The mathematical and experimental problems to solve equation (13) have been discussed by Momber and Kovacevic [**14**]. Figure 4 shows the relation between the relative erosion depth and the energy dissipation parameter, calculated from equation (13). For $\Phi = 1$, $\chi(\Phi) = 1$ is obtained, which means that the dissipated energy has reached a critical value and the maximum possible erosion depth is achieved. Between $\Phi = 0$ and $\Phi = 1$, the relation is non-linear and progressively increasing. It can be approximated by a second-order polynomial

$$\chi(\Phi) = A_1\Phi^2 + B_1\Phi + C_1 \tag{14}$$

where A_1, B_1 and C_1 depend on the process and material parameters. Interestingly, this type of approximation was also found in reference [**15**] for the relation between the depth of cut and the absolute dissipated energy in cast iron samples. A second-order polynomial was also successfully used in reference [**9**] to relate the peak amplitude of the striations generated during abrasive water jet cutting and the depth of cut. This behaviour seems to be realistic considering that the energies dissipated by friction and damping are very low for shallow erosion depths but

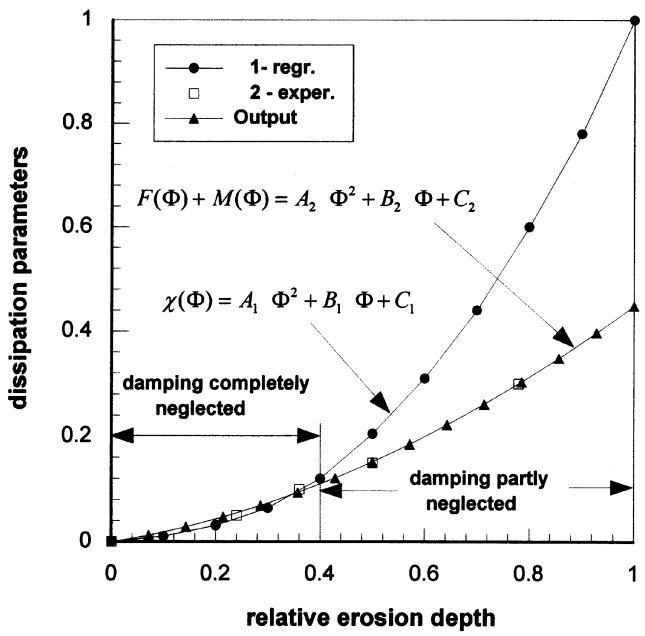

Fig. 4 The relation between the relative erosion depth and energy dissipation parameters, based on striation measurements and force measurements

contribute significantly to the dissipation process with increasing erosion depth. Nevertheless, equation (14) does not give information on the particular energy portions dissipated by erosion debris formation, wall friction and film damping. The following section contains some experimental methods developed by the present authors to estimate these particular energy losses.

4 ESTIMATION OF THE ENERGY DISSIPATION DUE TO FRICTION, DAMPING, EROSION AND DEBRIS FORMATION

4.1 Force measurements

It is assumed that, in the case of cutting through (characterized by the subscript T) of a thin specimen, damping effects due to a water–particle film can be neglected since the suspension leaves the erosion site at the bottom exit. This may be acceptable in the smooth cutting zone where the curvature of the striation can be neglected. Under the given conditions, this thickness was about $\Phi < 0.4$. The difference between the energy of the exiting suspension and the energy of the incoming high-speed slurry and the ratio of these two terms are then expressions for the energy dissipated due to wall friction and erosion debris formation respectively. Thus,

$$E_{\mathrm{M}} + E_{\mathrm{F}} = E_{\mathrm{S}} - E_{\mathrm{ex,T}} \tag{15}$$

For $\Phi = 1$, $E_{\mathrm{ex,T}} = E_{\mathrm{ex}}$. Alternatively,

$$M + F = 1 - \frac{E_{\mathrm{ex,T}}}{E_{\mathrm{S}}} \tag{16}$$

Assuming that the mass flowrate of the suspension is constant during the erosion process (the mass flow of the removed erosion debris is very low compared with the high-speed suspension) and considering the kinetic energy of a high-speed slurry according to equation (2), the ratio of the exit energy to the input energy can be expressed as a ratio of the square velocities and a ratio of the measured forces respectively. The force of a high-speed slurry is given by its impulse flow:

$$F_{\mathrm{S}} = \dot{I}_{\mathrm{S}} = (\dot{m}_{\mathrm{P}} + \dot{m}_{\mathrm{W}})v_{\mathrm{S}} \tag{17}$$

Equations (16) and (17) give

$$M(\Phi) + F(\Phi) = 1 - \left[\frac{v_{\mathrm{ex,T}}(\Phi)}{v_{\mathrm{S}}}\right]^2 = 1 - \left[\frac{F_{\mathrm{ex,T}}(\Phi)}{F_{\mathrm{S}}}\right]^2 \tag{18}$$

In order to measure the vertical force exerted by the jets, a four-component piezoelectric dynamometer was employed. The measuring platform is fitted with quartz cells. The

cells respond to the pressure exerted on the measuring platform by undergoing displacements. This response is converted to an electric charge proportional to the force component. The electric charge produced is supplied to a charge amplifier which converts the proportional voltage.

A typical plot of a measured force generated by a high-speed abrasive–water slurry during the erosion process is given in Fig. 5. Here, the left signal corresponds to level 1 in Fig. 1, the centre signal corresponds to level 2 in Fig. 1 and the right signal corresponds to level 3 in Fig. 1. A large amount of noise can be seen in this figure. The standard deviations of the acquired force signals are between 33 per cent for the abrasive water jet before cutting, and 37 per cent for the jet during cutting. There are several reasons for these deviations, mainly fluctuations in the pump pressure and the abrasive particle delivery and the unsteady localized material erosion. For further treatment, the signals have been averaged directly by commercial force signal analysis software.

The cutting through of several samples with different thicknesses (the sample thickness is assumed to be the erosion depth) and measuring the forces of the exiting slurry (level 3 in Fig. 1) gives the relation between the relative erosion depth and the energy dissipated owing to friction and erosion debris generation. The maximum possible erosion depth was simply estimated by a kerfing test under the given erosion conditions. The results of such experiments are shown in Fig. 4. The result can be approximated by a second-order polynomial

$$M(\Phi) + F(\Phi) = A_2\Phi^2 + B_2\Phi + C_2 \tag{19}$$

The function shows only a small non-linearity and, for $\Phi > 0.4$, the ordinate values are lower than the dissipation values estimated from the striation geometry. This is an expected result; the difference is the amount of energy dissipated by film damping. Also, as originally assumed, the difference between both functions is negligible in the range $\Phi < 0.4$. Beyond this value, the difference increases progressively, illustrating that damping effects become significant as the striation formation is introduced. The function

$$\begin{aligned} D(\Phi) &= \chi(\Phi) - M(\Phi) - F(\Phi) \\ &= (A_1 - A_2)\Phi^2 + (B_1 - B_2)\Phi + (C_1 - C_2) \end{aligned} \tag{20}$$

expressing the dissipation due to damping, is illustrated later in Fig. 9. Here, A_1, B_1 and C_1 are from the striation measurements, and A_2, B_2 and C_2 are from the force measurements. The function is excessively increasing with an increase in erosion depth. For $\Phi < 0.4$, damping can be neglected. This is, as already pointed out, due to the 'straight-line' geometry of the cutting front. This situation changes as the cutting front starts to incline. The abrasive particles now hit water-covered surfaces directly. Therefore, beyond $\Phi = 0.4$, damping effects come in front dramatically. For the case of kerfing ($\Phi = 1$), about 42 per cent of the dissipated energy is absorbed by damping. This is in agreement with results from dry solid–particle erosion. Clark and Burmeister [**16**] found for quartz particles suspended in water that about 33 per cent of the kinetic energy of the solid particles is required to penetrate a fluid film between the impinging particles and the target.

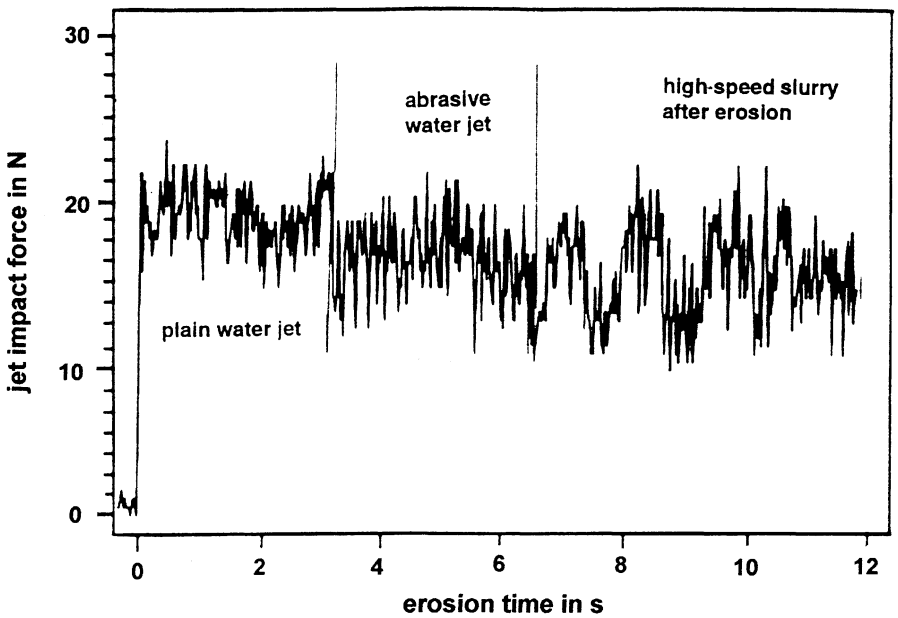

Fig. 5 A typical force signal detected by a dynamometer during the cutting of aluminium plates by a high-speed abrasive water jet

4.2 Material removal experiments

It can be assumed that a certain amount of the kinetic slurry energy is required to remove a certain amount of material during the erosion. This energy is E_M. To estimate this particular part of the dissipated energy, the two different experiments discussed below are suggested.

The first experiment (Fig. 6a) is based on the assumption that, for quasi-brittle pre-cracked materials, the general failure mechanisms during the compression test and the abrasive water jet erosion are similar. This has been experimentally proven in reference [**17**]. Therefore, the energy that is dissipated during the removal of a certain volume of material is equal to the specific fracture energy of the material. In the engineering literature, the specific fracture energy is often referred to as the area under the stress–strain curve of the given material under compression or tension. Thus,

$$E_M = E_{fr} V_M = M E_{diss} \tag{21}$$

The volume removed during abrasive water jet erosion is

$$V_M = h[\beta f(h)]L \tag{22}$$

For a small erosion depth and for a high-strength material, $f(h) \to 1$. Equations (21) and (22) give the amount of energy dissipated by fracture processes during the erosion debris formation. For $\Phi = 1$,

$$M = \frac{E_{fr}\beta L h_{max}}{K(p - p_{thr})} \tag{23}$$

The stress–strain curves of engineering materials are complex and, as abrasive water jet erosion experiments on rocks have shown, a simplification of the curves yields unsatisfactory results [**18**]. In this paper, the present authors used concrete samples for the investigations. The stress–strain curves were estimated by loading and unloading the specimens 11 times under compression. By integrating the resulting stress–strain functions between $\varepsilon = 0$ and the ultimate strain $\varepsilon = \varepsilon_{ult}$, the specific fracture energy was estimated:

$$E_{fr} = \int_0^{\varepsilon_{ult}} [\Theta(\varepsilon - \varepsilon_{ult})^2 + \sigma_{ult}]\, d\varepsilon \tag{24}$$

Here, $\Theta \approx 0.12$ is a dynamic loading parameter. The energy dissipation parameter M was calculated using equation (23) based on kerfing experiments. Thus, $\Phi = 1$. After kerfing, the depth, width and length of the cut have been measured to estimate the removed volume. For the experimental conditions, see Table 1.

Some results are shown in Fig. 7. The estimated values are between $M = 0.0002$ and $M = 0.0012$ and depend on the material properties. M increases almost linearly with increasing concrete strength parameters. Under compression as well as under abrasive water jet erosion, the samples with higher strengths show a more brittle behaviour, which leads to larger fracture debris and to transcrystalline fractures. This was verified by inspections of the fracture debris and the erosion sites via optical microscopy. The same tendency was independently noticed in reference [**17**] based on acoustic emission measurements. Also, M decreases as the pump pressure increases and the traverse rate decreases. Therefore, a higher kinetic slurry energy leads to worse energy transfer in the erosion debris formation process.

The second experiment (Fig. 6b) is based on the assumption that the energy required for creating new surfaces (of the erosion debris) in specimens of brittle behaviour is proportional to the work of fracture of a material. The model of Zeng and Kim [**19**] for the abrasive

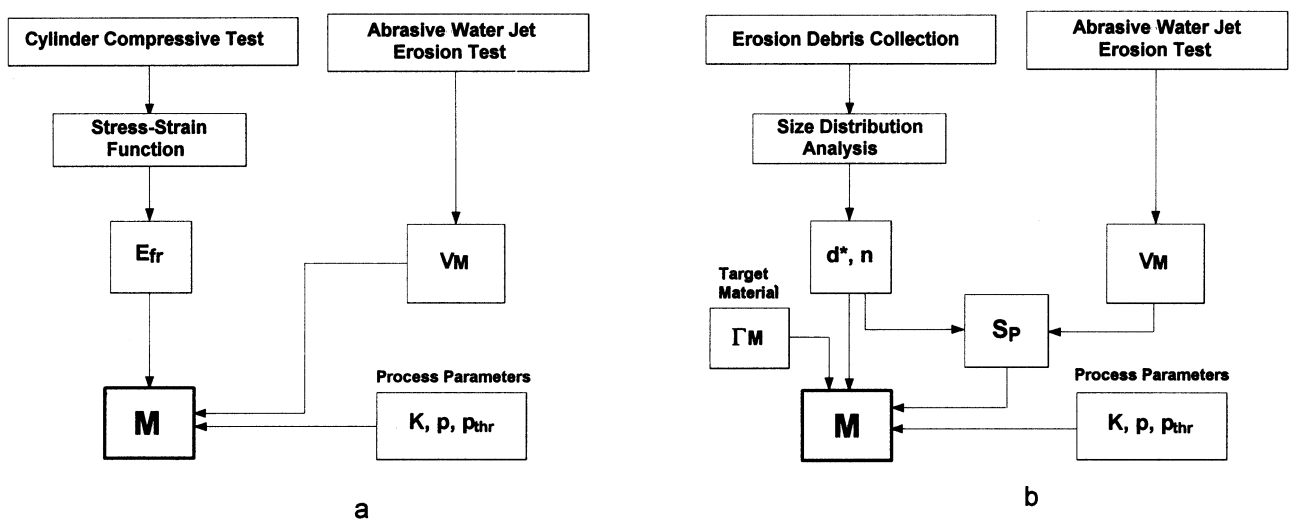

Fig. 6 Schematic diagrams of the experimental estimation of the dissipation parameter M for erosion debris formation

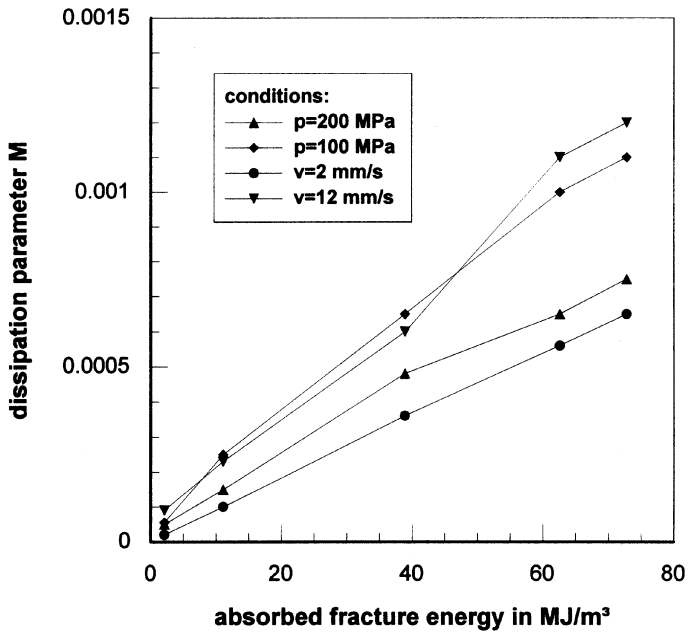

Fig. 7 The relation between the absorbed fracture energy of concrete specimens and the energy dissipation parameter $M(\Phi)$, based on compressive fracture experiments (concrete)

water jet erosion of brittle material, which gives the generation of a microcrack network on the erosion site, supports this assumption. Thus, the energy dissipated during the generation of the erosion debris is approximately given by

$$E_{\mathrm{M}} = 2\Gamma_{\mathrm{M}} S_{\mathrm{P}} = M E_{\mathrm{diss}} \tag{25}$$

It was shown in a previous investigation that the particle size distribution of erosion debris removed from materials with mainly brittle behaviour follows a Rosin–Rammler–Sperling (RRSB) distribution [**20**]. This enables the surface of the erosion debris sample to be approximated by using the RRSB distribution parameters d^* and n [**21**]:

$$S_{\mathrm{P}} = \frac{6.39\,\mathrm{e}^{1.769/n^2}\,V_{\mathrm{M}}}{d^*} \tag{26}$$

Equations (25) and (26) give

$$M = \frac{\Gamma_{\mathrm{M}} \times 11.62\,\mathrm{e}^{1.769/n^2}\,V_{\mathrm{M}}}{d^* K(p - p_{\mathrm{thr}})} \tag{27}$$

The present authors used cast iron samples with a work of fracture $\Gamma_{\mathrm{M}} = 4500\ \mathrm{J/m^2}$ for the erosion experiments. Again, kerfing experiments were carried out. Thus, $\Phi = 1$. The removed erosion debris were collected, separated by a magnetic method and analysed by sieving. The distribution parameters d^* and n were estimated graphically using a special distribution diagram. For the experimental conditions, see Table 1.

Some examples of calculated M values are plotted in Fig. 8. For the given process conditions, values between $M = 0.017$ and $M = 0.024$ were found. This is an order of magnitude higher than the results obtained from equation (23). Interestingly, the trend that the efficiency of the material removal process decreases as the initial kinetic energy of the impacting slurry flow increases is observed again, at least if a certain energy value is exceeded. The higher the impact velocity, the lower are the values for M. Also, the considerably higher values for M found in this experiment may partly be caused by the extremely high resistance of the cast iron material used. As already illustrated in Fig. 7, the efficiency is high if the strength parameters of the target material have high values. On the other hand, the quantitative differences in the experimental results of both methods may be due to the differences in the process conditions, the experimental procedures and the target material response.

If the experiments described in Section 4 and the force measurements performed in Section 4.1 are carried out under identical process conditions, the energy dissipation parameter F can be approximated by

$$\begin{aligned} F(\Phi) &= [F(\Phi) + M(\Phi)] - M(\Phi) \\ &= (A_2\Phi^2 + B_2\Phi + C_2) - M(\Phi) \end{aligned} \tag{28}$$

but, because of the experimental restrictions in the material removal experiments (kerfing), equation (28) is valid only for $\Phi = 1$. As Fig. 9 shows, the energy dissipation due to

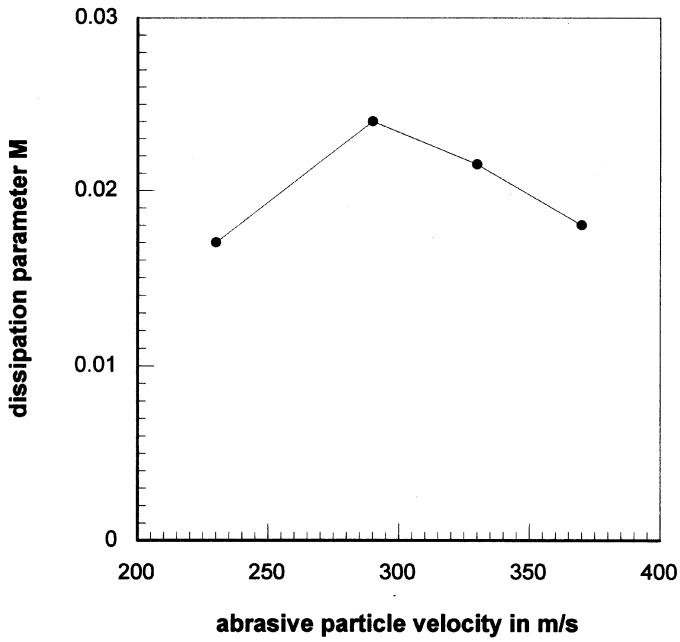

Fig. 8 The relation between the velocity of the high-speed abrasive–water flow and the energy dissipation parameter $M(\Phi)$, based on debris analysis (cast iron)

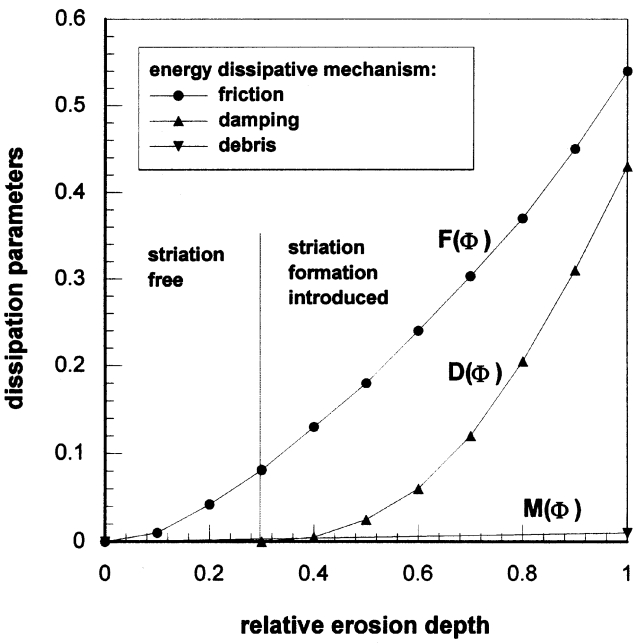

Fig. 9 Energy dissipation during the erosion of materials by a high-speed abrasive–water flow

friction tends to increase with increasing erosion depth. The increase is non-linear, but the non-linearity is not as pronounced as it is in the case of damping. Also, even in the range $\Phi < 0.4$, significant friction can be noticed. Therefore, friction seems to be almost independent of the curvature of the cutting front. For the case of kerfing ($\Phi = 1$), about 53 per cent of the energy dissipated in the workpiece is due to friction.

5 CONCLUSIONS

1. The energy dissipated during the material erosion by a high-speed abrasive–water flow is investigated in this study. It is shown by a simple physical–mathematical model and by experiments that the energy dissipation can be expressed as a function of the relative erosion depth.
2. In order to separate the physical components of the energy dissipation function, experimental methods were developed and applied. For the estimation of the energy dissipation due to damping $D(\Phi)$, force measurements were carried out on the high-speed slurries during the erosion process. For the calculation of the energy dissipated during the erosion debris formation $M(\Phi)$, fracture experiments as well as grain size distribution experiments were performed. The energy dissipated by friction $F(\Phi)$ has been estimated as the difference between the global energy dissipation function and the experimentally measured functions $M(\Phi)$ and $D(\Phi)$.
3. By combining the mathematical–physical model and the experimental methods developed, it is possible to estimate the complete energy dissipation characteristics of the high-speed erosion.
4. Figure 9 shows a comparison between the dissipation processes discussed in this paper. The plotted values, especially in the range $0.4 < \Phi < 1$, are just rough approximations. Nevertheless, for the first time, they give a feeling about the energy situation in a workpiece cut by the erosive action of high-speed abrasive water jets.

ACKNOWLEDGEMENT

The authors are grateful to the Alexander von Humboldt-Foundation, Bonn, Germany, for financial support.

REFERENCES

1 **Momber, A. W., Eusch, I.** and **Kovacevic, R.** Machining refractory ceramics by abrasive water jets. *J. Mater. Sci.*, 1996, **31**, 6485–6493.
2 **Arola, D.** and **Ramulu, M.** Micro-mechanisms of material removal in abrasive waterjet machining. *Proc. Advanced Mater.*, 1994, **4**, 37–47.
3 **Momber, A. W.** and **Kovacevic, R.** *Principles of Abrasive Water Jet Machining*, 1998 (Springer-Verlag, London).
4 **Momber, A. W.** and **Kovacevic, R.** Test parameter analysis in abrasive water jet cutting of rocklike materials. *Int. J. Rock Mechanics Min. Sci.*, 1997, **34**, 17–25.
5 **Hashish, M.** Visualization of the abrasive-waterjet cutting process. *Exp. Mechanics*, 1988, **28**, 159–169.
6 **Blickwedel, H.** Erzeugung und Wirkung von Hochdruck-Abrasivstrahlen. PhD thesis, University of Hannover, 1990.
7 **Raju, S. P.** and **Ramulu, M.** Predicting hydro-abrasive erosion wear during abrasive water jet cutting. In *Manufacturing Science and Engineering*, 1994, pp. 339–351 (American Society of Mechanical Engineers, New York).
8 **Zhou, G., Geskin, E. S.** and **Chung, Y. C.** Investigation of topography of waterjet generated surfaces. 1991, PED-Vol. 62, pp. 191–202 (American Society of Mechanical Engineers, New York).
9 **Chao, J.** and **Geskin, E. S.** Experimental study of the striation formation and spectral analysis of the abrasive generated surfaces. In Proceedings of the Seventh American Water Jet Conference, Seattle, Washington, 1993, pp. 27–41.
10 **Guo, N. S., Louis, H.** and **Meier, G.** Surface structure and kerf geometry in abrasive water jet cutting: formation and optimization. In Proceedings of the Seventh American Water Jet Conference, Seattle, Washington, 1993, pp. 1–25.
11 **Momber, A. W.** and **Kovacevic, R.** Energy dissipative processes in high speed water-solid particle erosion. In Proceedings of the ASME Heat Transfer and Fluids Engineering Division, 1995, pp. 243–256 (American Society of Mechanical Engineers, New York).
12 **Momber, A. W.** and **Kovacevic, R.** Calculation of exit jet energy in abrasive water jet cutting. In *Manufacturing Science*

and Engineering, 1994, pp. 361–366 (American Society of Mechanical Engineers, New York).

13 **Zeng, J., Hines, R.** and **Kim, T. J.** Characterization of energy dissipation phenomena in abrasive water jet cutting. In Proceedings of the Sixth American Water Jet Conference, Houston, Texas, 1991, pp. 163–177.

14 **Momber, A. W.** and **Kovacevic, R.** Quantification of energy absorption capability in abrasive water jet machining. *Proc. Instn Mech. Engrs, Part B, Journal of Engineering Manufacture*, 1995, **209**(B6), 491–498.

15 **Mohan, R. S., Momber, A. W.** and **Kovacevic, R.** Detection of energy absorption during abrasive water jet machining using acoustic emission technique. In *Manufacturing Science and Engineering*, 1995, pp. 69–85 (American Society of Mechanical Engineers, New York).

16 **Clark, H. M.** and **Burmeister, L. C.** The influence of the squeeze film on particle impact velocities in erosion. *Int. J. Impact Engng*, 1992, **12**, 415–426.

17 **Momber, A. W., Mohan, R. S.** and **Kovacevic, R.** On-line analysis of hydro-abrasive erosion of pre-cracked materials by acoustic emission. *Theor. Appl. Fracture Mechanics*, 1999, **31**, 1–17.

18 **Matsui, S., Matsumura, H., Ikemoto, Y., Kumon, Y.** and **Shimizu, H.** Prediction equations for depth of cut made by abrasive water jet. In Proceedings of the Sixth American Water Jet Conference, Houston, Texas, 1991, pp. 31–41.

19 **Zeng, J.** and **Kim, T. J.** Development of an abrasive waterjet kerf cutting model for brittle materials. *Jet Cutting Technology*, 1992, pp. 483–501 (Kluwer, Dordrecht).

20 **Momber, A. W., Kwak, H.** and **Kovacevic, R.** Investigations in abrasive water jet erosion based on wear particle analysis. *Trans. ASME, J. Tribology*, 1997, **118**, 759–766.

21 **Kiesskalt, S.** and **Matz, G.** Zur Ermittlung der spezifischen Oberfläche von Kornverteilungen. *VDI-Z.*, 1951, **58**, 58–60.

